Ionic liquids containing half-sandwich ruthenium complexes: in situ interconversions via photochemical and thermal ligand exchange

Mochida, Tomoyuki
Maekawa, Syou
Sumitani, Ryo

(Citation)
New Journal of Chemistry,47(41):19096-19102

(Issue Date)
2023-11-07

(Resource Type)
journal article

(Version)
Accepted Manuscript

Ionic liquids containing half-sandwich ruthenium complexes: in-situ interconversions via photochemical and thermal ligand exchange†

Tomoyuki Mochida,*[a,b] Syou Maekawa,[a] and Ryo Sumitani[a]

[a]*Department of Chemistry, Graduate School of Science, Kobe University, Rokkodai, Nada, Kobe, Hyogo 657-8501, Japan. E-mail: tmochida@platinum.kobe-u.ac.jp*

[b]*Research Center for Membrane and Film Technology, Kobe University, Rokkodai, Nada, Kobe, Hyogo 657-8501, Japan*

†Electronic supplementary information (ESI) available. See DOI: https://

Abstract

Cyclopentadienyl (Cp) Ru complexes exhibit diverse chemical reactivity and are versatile as catalysts, but their applications to functional materials are yet to be explored. To develop stimuli-responsive liquids based on their reactivity, Ru-containing ionic liquids (ILs) $[Ru(Cp)L^1L]Tf_2N$ (L^1 = *N*-hexyl-2-pyridinemethanimine; L = CO, MeCN, SMe_2, and DMSO) were synthesized in this study. Their colors, physical properties, and chemical reactivities were dependent on the auxiliary ligand L, and these ILs exhibited interconversions via in-situ ligand exchange. The exchange from CO to other ligands occurred via UV photoirradiation, whereas the other ligand exchange reactions occurred thermally. On the other hand, $[Ru(Cp)L^2(CO)]Tf_2N$ (L^2 = *N*-Methyl-*N*-hexyl-2-pyridinemethanamine) did not undergo photochemical ligand exchange.

Introduction

Cationic cyclopentadienyl (Cp) Ru complexes constitute a distinct area in organometallic chemistry because of their diverse chemical reactivities and catalytic abilities.[1] In particular, sandwich-type CpRu-arene complexes exhibit intriguing photoreactivity, which is useful for synthetic reactions and photofunctional applications. Although a number of half-sandwich CpRu complexes such as those with *N*,*N*-chelate ligands have been reported to date,[2] their photochemistry and application in functional materials have been less explored.

Ionic liquids (ILs) are salts with low melting points, which typically comprise quaternary cations and fluorinated anions. ILs have been studied for various applications, such as electrolytes, solvents, gas absorbents, and catalysts due to their high ionic conductivities, negligible vapor pressures, and solubilizing abilities.[3] Furthermore, various functional ILs containing metal ions have been reported.[4-6] We have synthesized a variety of ILs containing cationic sandwich and half-sandwich complexes.[7,8] In particular, half-sandwich complexes are diverse in structure and reactivity, endowing ILs with various functionalities, such as catalytic activity,[9] ligand exchange,[10,11] and linkage isomerization,[12] though they are often irreversible. Development of reactive organometallic ILs leads to novel applications of organometallic compounds.

In this study, to develop stimuli-responsive ILs exhibiting reversible conversions, we synthesized CpRu complexes with *N*,*N*-chelate ligands (L^1 = *N*-hexyl-2-pyridinemethanimine, L^2 = *N*-methyl-*N*-hexyl-2-pyridinemethanamine; Fig. 1a) and investigated their physical properties and chemical reactivities. The ligands were chosen considering the ligand exchange abilities of $[Ru(Cp)(tmeda)]^+$ (tmeda = *N*,*N*,*N*',*N*'-tetramethyl-1,2-ethanediamine),[13] and the bis(trifluoromethane)sulfolylamide anion (Tf_2N^-) was used as the counter anion. Hence, the L^1-containing ILs $[Ru(Cp)L^1L]Tf_2N$ (**1-L**; L = CO, MeCN, SMe_2, and DMSO) were revealed to exhibit reversible auxiliary ligand exchange, leading to conversion between ILs that differ

in color, physical properties, and reactivities. In particular, the ligand exchange from the carbonyl complex occurred photochemically, featuring an unprecedented photoinduced CO release from the CpRu complexes. In contrast, the use of L^2 resulted in the isolation of only $[Ru(Cp)L^2(CO)]Tf_2N$ (**2-CO**), which did not undergo ligand exchange. The physical properties of the ILs were also compared with those of the previously reported $[Ru(C_6H_6)(NCS)L^1]Tf_2N$ (**3**, Fig. 1b), which represents an IL undergoing irreversible linkage isomerization of the thiocyanate ligand.[12]

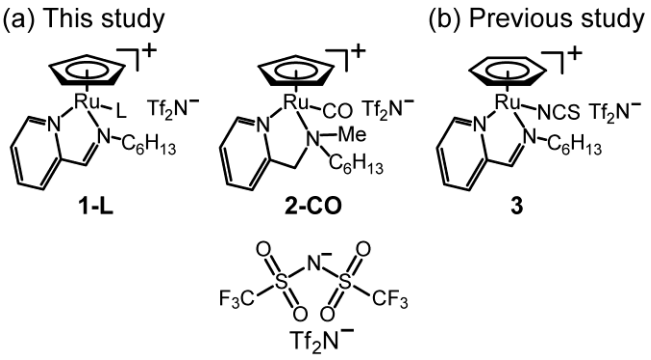

Fig. 1. Structural formulas of (a) Ru-containing ILs **1-L** (L = CO, SMe_2, DMSO, MeCN) and **2-CO** synthesized in this study and (b) $[Ru(C_6H_6)(NCS)L^1]Tf_2N$ (**3**).[12] The structure of the Tf_2N anion is also shown.

Results and Discussion

Synthesis and properties

The synthesis procedure of **1-L** is shown in Fig. 2. The reaction of $[Ru(Cp)(MeCN)_3]PF_6$ with L^1 produced a solid PF_6 salt with a MeCN ligand, the structure of which was confirmed by X-ray crystallography at 90 K (Fig. 3). **1-MeCN** was synthesized from the PF_6 salt by anion exchange, which was obtained as a solid but maintained the liquid state at room temperature after melting (T_m = 339 K). The reaction of this IL with carbon monoxide in dichloromethane produced liquid **1-CO**. The dissolution of **1-MeCN** in dimethyl sulfide or dimethyl sulfoxide, followed by solvent evaporation, quantitatively yielded liquid **1-SMe_2** and solid **1-DMSO**,

and the latter maintained liquid state at room temperature after melting (T_m = 345 K). **2-CO** was obtained as a liquid due to the reaction of $[Ru(Cp)(MeCN)_3]PF_6$ with L^2 and carbon monoxide, followed by anion exchange, whereas **2-MeCN** could not be isolated because of its instability.

The UV–Vis spectra and photographs of the ILs in the liquid state, sandwiched between quartz plates, are shown in Fig. 4. The colors of the ILs changed remarkably depending on the ligands, which were consistent with the UV–Vis spectra. **1-SMe2** and **1-MeCN** appeared brown and **1-DMSO** was orange, while **1-CO** and **2-CO** appeared yellow and pale yellow, respectively, when sandwiched between quartz plates. However, the colors of the bulk liquids looked much darker and more brownish to the naked eye. The DFT calculations of the cations in these salts showed an increase in their HOMO–LUMO gaps with values of 7.0, 7.0, 7.4, 7.6, and 8.6 eV, respectively. The results of TD-DFT calculations were consistent with the observed tendency (Figure S4), which revealed that the dominant absorption peaks are HOMO–LUMO or similar transitions.

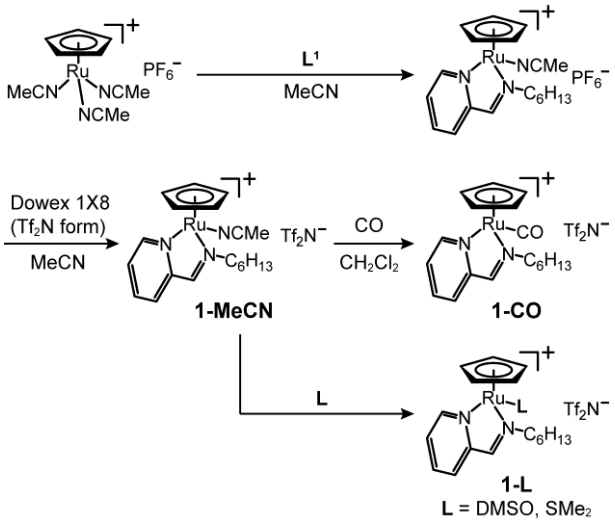

Fig. 2. Synthetic schemes of **1-L** (L = MeCN, CO, SMe_2, and DMSO).

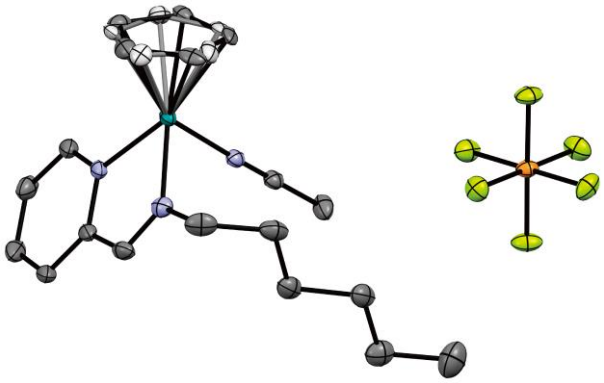

Fig. 3. Molecular structure of [Ru(Cp)L^1(MeCN)]PF_6. Hydrogen atoms are omitted. The Cp ring is disordered, and the less occupied part is shown with a lighter color.

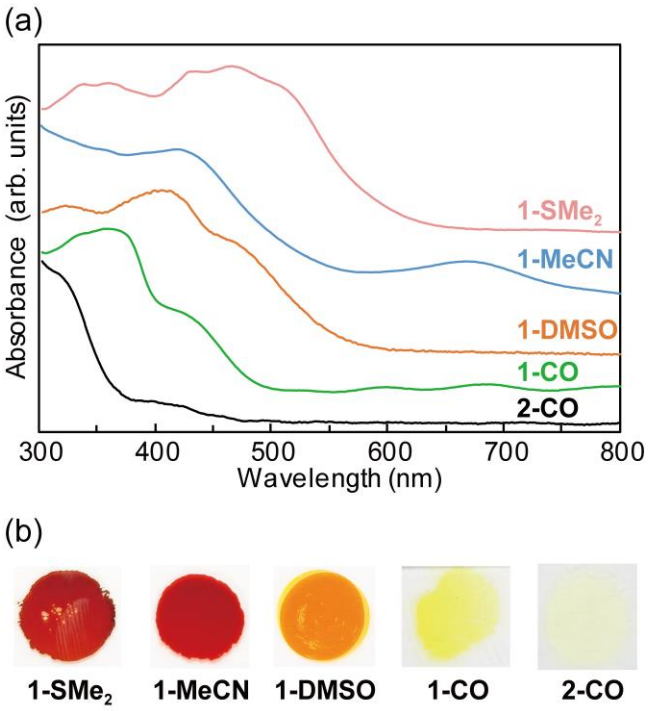

Fig. 4. (a) UV–Vis spectra of **1-L** (L = SMe_2, MeCN, DMSO, and CO) and **2-CO** in the liquid state. The spectra are vertically shifted for clarity. (b) Photographs of the ILs sandwiched between quartz plates.

Thermal properties

The thermal properties of the synthesized ILs were investigated by DSC and TG-DTA, and the obtained melting points (T_m), glass transition temperatures (T_g), and decomposition

temperatures (T_{dec}) are listed in Table 1.

Solid **1-MeCN** and **1-DMSO** melted at 338.9 K (ΔH = 28.3 kJ mol^{-1}) and 345.2 K ((ΔH = 29.8 kJ mol^{-1}), respectively. These salts remained in a liquid state at ambient temperature after melting and showed glass transition at 236 and 250 K, respectively, upon cooling. The values of T_g/T_m were 0.70 and 0.72, respectively, which agree with the empirical relationship T_g/T_m = 2/3 for molecular liquids.[14] **1-SMe$_2$**, **1-CO**, and **2-CO** exhibited glass transitions at 227, 235, and 238 K, respectively, which are considerably lower than that of **3** (T_g = 273 K).[12]

The TG measurements of the ILs were performed to examine their thermal decomposition behavior (sweep rate: 3 K min^{-1}, Fig. 5 and Fig. S5†). **1-MeCN** and **1-SMe$_2$** exhibited similar decomposition temperatures (−3 wt%), approximately 438 K, indicating that both ligands were coordinated with similar strength, which is consistent with their mutual conversion described above. **1-DMSO** exhibited higher decomposition temperature at 462 K, which agrees with the high coordination ability of DMSO. In each case, continuous mass loss due to the ligand desorption and decomposition was observed, suggesting that the isolation of the 16-electron complex via thermal desorption of the ligand is not feasible.

The decomposition temperatures of **1-CO** and **2-CO** (−3 wt%) were 525 and 476 K, respectively. As expected, they were thermally more robust than **1-L** (L = MeCN, SMe_2, and DMSO) owing to the strong coordination of CO ligands.

Table 1. Melting points (T_m), glass transition temperatures (T_g), and decomposition temperatures (T_{dec}) of synthesized ILs and related materials

	T_m (K)	T_g (K)	T_{dec} (K)[a]
1-MeCN	338.9	236	438
1-SMe$_2$		227	439
1-DMSO	345.2	250	462
1-CO		235	525
2-CO		238	476

3[b,c]	273	435

[a]Determined by TG (−3% wt). [b]Ref. 12. [c]Mixture of *N*- and *S*-coordinated isomers in a 0.7:0.3 ratio.

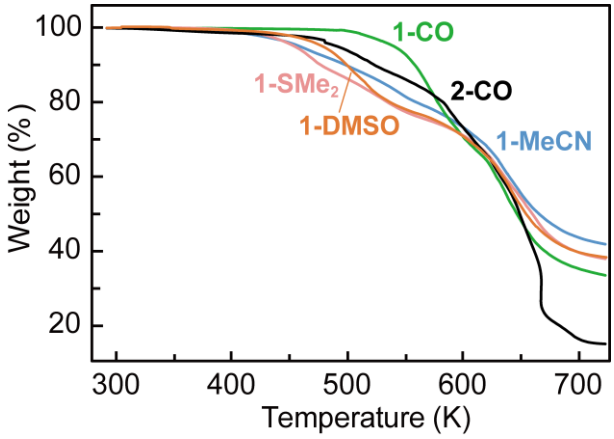

Fig. 5. TG curves of **1-L** (L = SMe_2, MeCN, DMSO, and CO) and **2-CO** measured under dinitrogen atmosphere (3 K min^{-1}).

Viscosity

The temperature dependence of the viscosities of the ILs is shown in Fig. 6. The viscosity values for **1-MeCN** and **1-DMSO** are plotted above their melting points. The viscosities of each IL at 298 (η_{298K}) and 353 K (η_{353K}) are listed in Table 2. Each IL behaved as a Newtonian liquid.

1-MeCN, **1-DMSO**, and **2-CO** were highly viscous liquids with similar viscosity values, whereas **1-SMe2** and **1-CO** have less viscosity (Fig. 6). The viscosities of these ILs (e.g. η_{298K} = 2.9 Pa·s (**1-CO**), 10.9 Pa·s (**2-CO**)) were two orders of magnitude larger than those of typical ILs, such as [Emim]Tf_2N (Emim = 1-ethyl-3-methylimidazolium; $\eta_{298K} = 4.2 \times 10^{-2}$ Pa s).[15] However, they were three orders of magnitude less viscous than **3** ($\eta_{298K} = 7.9 \times 10^3$ Pa s, T_g = 273 K),[12] which is consistent with their lower glass transition temperatures (T_g = 227–238 K).

The tendencies observed in the thermal properties and viscosities of the ILs were

consistent with their cation shapes (Fig. 7). The cations in **1-SMe$_2$** and **1-CO** are closer to spherical, accounting for their low viscosity and low glass transition temperatures. In contrast, the cations in **1-MeCN** and **1-DMSO** encounter higher steric hindrance from the ligands, leading to their high melting points. **2-CO** also has steric hindrance owing to the additional methyl group in L^2.

The temperature dependence of the viscosities was fitted using the Vogel–Fulcher–Tammann (VFT) equation ($\eta = \eta_0 e^{(DT_0/(T-T_0))}$)[16] and the Andrade equation ($\eta = \eta_0 e^{(E_a/RT)}$),[17] and the fitting parameters are listed in Table 2. Each IL has smaller E_a and D values compared with **3**.

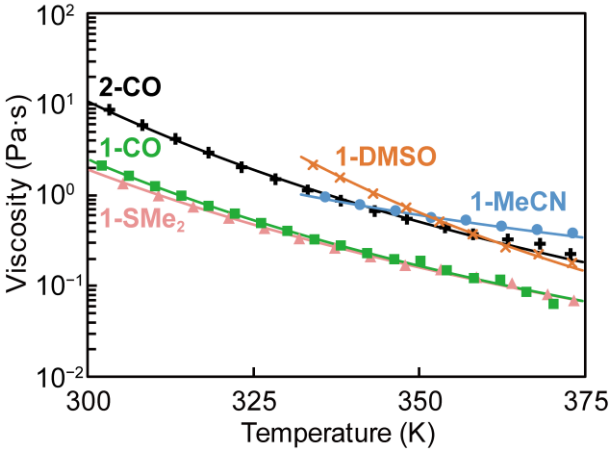

Fig. 6. Temperature dependence of the viscosities of **1-L** (L = SMe_2, MeCN, DMSO, and CO) and **2-CO** (shear rate 1 s^{-1}). The curves are fitted using the VFT equation.

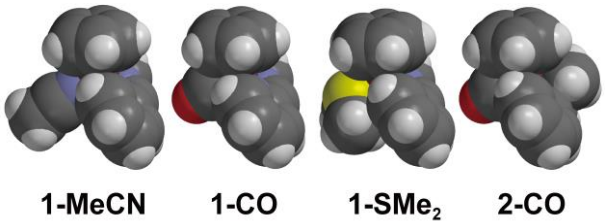

Fig. 7. Cation shape of **1-L** (L = MeCN, CO, SMe_2) and **2-CO** obtained using DFT calculations (ωB97-D/LanL2DZ). Hexyl groups are substituted with methyl groups.

Table 2. Viscosities and fitting parameters of synthesized ILs and related materials

	η_{298K} (Pa s)	η_{353K} (Pa s)	D^a	T_0 (K)^a	η_0 (Pa s)^a	E_a (kJ mol^{-1})^b
1-MeCN^c	(0.79)^d	0.53	4.6(2.2)	175.3(27.9)	6.1(4.4) × 10^{-3}	63.7
1-SMe$_2$	2.04	0.14	15.6(2.6)	125.4(8.8)	2.7(1.4) × 10^{-5}	46.0
1-DMSO^c	(1.59)^d	1.24	7.8(1.0)	200.3(6.7)	1.9(1.1) × 10^{-5}	67.3
1-CO	2.86	0.15	11.0(2.0)	149.2(9.5)	4.8(2.8) × 10^{-5}	45.6
2-CO	10.9	0.36	14.6(0.5)	140.2(1.7)	3.0(0.4) × 10^{-5}	53.9
3^{e,f}	7900	7.58	22.0(1.4)	158.1(3.2)	1.37(0.72) × 10^{-7}	107.6

^{a}Parameters for the VFT equation. ^{b}Activation energy based on the Andrade equation. ^{c}Fitting above 338 K (T_m). ^{d}Value at 338 K. ^{e}Ref. 12. ^{f}Mixture of *N*- and *S*-coordinated isomers in a 0.7:0.3 ratio.

Interconversions between ILs

1-L (L = MeCN, SMe_2, DMSO, and CO) exhibited quantitative interconversion (Fig. 8). As stated in the synthesis section, the dissolution of **1-MeCN** in excess dimethyl sulfide or dimethyl sulfoxide, followed by solvent evaporation, quantitatively yielded **1-SMe$_2$** and **1-DMSO**. The reverse reactions and the reactions between **1-SMe$_2$** and **1-DMSO** occurred in a similar manner. Liquids of **1-L** (L = MeCN, SMe_2, and DMSO) gradually transformed into **1-CO** under CO atmosphere, with a simultaneous color change from brown or brownish orange to yellow-orange. The reactions of **1-MeCN** and **1-DMSO** with CO completed within several hours at temperatures of several degrees higher than their melting points, whereas the reactions did not occur in the solid state. The reaction of **1-SMe$_2$** at 290 K was slow, completing within 2 days.

The conversion from **1-CO** to **1-L** (L = MeCN, SMe_2, and DMSO) occurred quantitatively within 5 min upon UV photoirradiation (365 nm) following the addition of MeCN, SMe_2, or DMSO. Excess ligands were removed either by evaporation or vacuum drying, taking advantage of the nonvolatility of ILs. Notably, these reactions occur via CO photodissociation. The molecular orbitals obtained using DFT calculations supported the photoreactivity of **1-CO** (Fig. S6†). The HOMO and the LUMO of **1-CO** showed bonding and weak bonding characteristics, respectively, with respect to the Ru–CO bond, which

supported CO dissociation upon photoexcitation. In contrast, the HOMO and LUMO of the cation of **1-MeCN** exhibited antibonding and nonbonding features, respectively, suggesting that the auxiliary ligand was not prone to photodissociation. The photochemical ligand exchange ability of the carbonyl ligand discovered in this study may be useful for the applications of CpRu complexes for chemical reactions and catalysis. Furthermore, the obtained results are significant since metal complexes exhibiting photoinduced CO release have attracted attention in recent times, especially from biomedicine.[18] Organometallic Ru complexes often demonstrate biological activities, such as antibacterial properties and cytotoxic activities,[19] hence, the introduction of CO releasing properties, as discovered in this study, may expand their biological applicability.

In contrast to **1-CO**, ligand exchange from **2-CO** was not possible because it yielded decomposition products on UV photoirradiation in MeCN, SMe_2, or DMSO. This phenomenon may be ascribed to the photocleavage of the Ru–N_{amine} bond since DFT calculations suggested the bonding and antibonding properties of the HOMO and LUMO of **2-CO**, respectively, with respect to the Ru–N_{amine} bond. In addition, the optimized structure of the cation in **2-CO** had a longer Ru–N_{amine} bond (2.21 Å) than the other Ru–N bonds in **2-CO** or **1-L** (2.10–2.13 Å), indicating the weakness of the Ru–N_{amine} bond.

The reactivities of these complexes are compared with those of $[Ru(Cp)(tmeda)L]^+$. $[Ru(Cp)(tmeda)(MeCN)]^+$ produces a 16-electron complex $[Ru(Cp)(tmeda)]^+$ via MeCN dissociation upon heating under vacuum.[13] In contrast, heating **1-MeCN** under vacuum at 373 K mainly yielded decomposition products, although partial MeCN desorption was observed, which is consistent with the TG experiments described above. Further, the UV photoirradiation of **1-CO** and **2-CO** under vacuum caused negligible CO dissociation, failing to provide the 16-electron complexes. We confirmed that the UV photoirradiation of $[Ru(Cp)(tmeda)(CO)]^+$ in solution resulted in decomposition, similar to that of **2-CO**,

demonstrating that a conjugated ligand is needed for CO photodissociation. While $[Ru(Cp)(tmeda)]^+$ gave carbene(CH_2)-coordinated complexes in dichloromethane,[13] the dissolution of **1-MeCN** in dichloromethane gave only unidentifiable products.

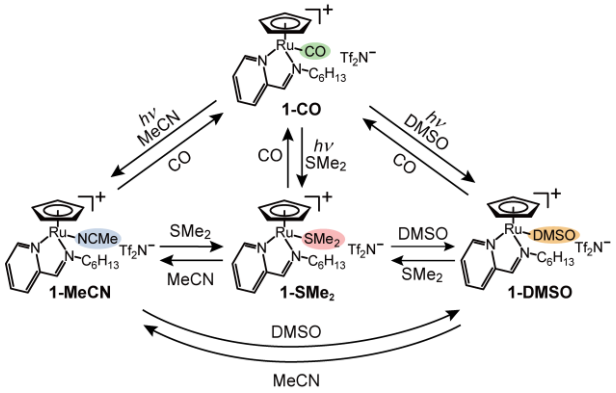

Fig. 8. Interconversion of **1-L** (L = SMe_2, MeCN, DMSO, and CO).

Conclusion

We synthesized ILs containing cationic CpRu half-sandwich complexes, each having a chelating ligand (L^1 or L^2) and an auxiliary ligand (L). The investigation of L^1-coordinated ILs revealed that the interconversions between them occur via in-situ ligand exchange, facilitating conversions between ILs that differ in color, physical properties, and reactivities. Particularly, the ligand exchange from CO to other ligands occurred photochemically. Thus, multiple conversion pathways between ILs with different auxiliary ligands were achieved. In the previously reported ILs containing half-sandwich complexes, conversions between structurally different ILs based on ligand exchange or linkage isomerization were irreversible.[10-12] On the other hand, only the CO-coordinated complex was isolated for L^2, which exhibited no photochemical ligand exchange, demonstrating notable reactivity dependence on the chelate ligand.

Ligand exchange is a prevalent reaction in organometallic complexes, offering significant advantages when applied to ILs. Their inherent liquid state permits reactions to proceed

solvent-free, and the nonvolatility of ILs enables the straightforward removal of excess reactants under vacuum. Although these are still proof-of-concept experiments, further investigation of reactive organometallic species for ILs will lead to the emergence of a new research area in liquid-state coordination chemistry. In terms of organometallic chemistry, the photoinduced CO release from the cationic CpRu chelate complex discovered in this study may improve their potential applications in chemical reactions, catalysts, and biomedicine. Mechanistic details of the photoinduced CO release are to be further investigated using spectroscopic methods in the near future.

Experimental

General

N-Hexyl-2-pyridinemethanimine (L^1) and *N*-methyl-*N*-hexyl-2-pyridinemethanamine (L^2) were synthesized as reported in the literature.[20] Other reagents were commercially available. ^{1}H NMR and ^{19}F NMR spectra were recorded using a Bruker Avance 400 spectrometer. IR spectra were recorded using a Thermo Nicolet iS5 with an ATR attachment. ESI-MS spectra were measured using a Thermo Fisher Scientific LTQ-Orbitrap Discovery. UV–Vis spectra were recorded on a JASCO V-570 UV–VIS/NIR spectrophotometer using liquid samples sandwiched between quartz plates. DSC was performed using a TA Instrument Q100 differential scanning calorimeter. Aluminum hermetic pans were used with a scanning rate of 10 K min^{-1}. TG-DTA was performed using a Rigaku TG8120 under nitrogen atmosphere, at a heating rate of 3 K min^{-1}. Viscosity measurements were performed using a TA Instrument DHR-2. UV photoirradiation was conducted using a Hamamatsu LC-L1 V3 lightning cure UV-LED (365 nm). DFT calculations were performed with a Spartan'20 (Wave function Inc.) at the ωB97-D/LanL2DZ level.

Synthesis

Synthesis of [Ru(Cp)L^1(MeCN)]PF$_6$. A solution of L^1 (125 mg, 0.658 mmol) in acetonitrile (5 mL) was added to [Ru(Cp)(MeCN)$_3$]PF$_6$ (263 mg, 0.606 mmol) and stirred for 2 h at ambient temperature under nitrogen atmosphere. The solvent was removed under reduced pressure, and the residue was purified using column chromatography (alumina, eluent: acetonitrile, R_f = 0.8). The recrystallization of the product from acetonitrile (213 K) yielded the desired product as dark brown crystals (288 mg, 89% yield). ^{1}H NMR (400 MHz, CD_3CN): δ = 0.92 (t, 3H, CH_3, J = 6.58 Hz), 1.27–1.42 (m, 6H, C_3H_6), 1.96 (s, 3H, $NCCH_3$), 2.01–2.12 (m, 2H, NCH_2CH_2), 4.16–4.52 (m, 2H, NCH_2), 4.45 (s, 5H, C_5H_5), 7.46–7.50 (m, 1H, 5-Pyr-CH), 7.91–7.96 (m, 2H, 3,4-Pyr-CH), 8.60 (s, 1H, N=CH), 9.37 (d, 1H, 6-Pyr-CH, J = 5.52 Hz). FT-IR (ATR, cm^{-1}): 556, 771, 828, 879, 933, 991, 1053, 1100, 1158, 1236, 1252, 1295, 1349, 1439, 1469, 1552, 1607, 2858, 2919. Anal. Calcd. for $C_{19}H_{26}F_6N_3PRu$: C, 42.07; H, 4.83; N, 7.75. Found: C, 42.19; H, 5.04; N, 7.74.

Synthesis of [Ru(Cp)L^1(MeCN)]Tf$_2$N (1-MeCN). Anion exchange resin (Dowex 1X8, 7.5 g), charged with Tf_2N anion using an aqueous solution of KTf_2N, was placed in a column and eluted using acetonitrile (100 mL). The column was then charged with an acetonitrile solution (5 mL) of [Ru(Cp)L^1(MeCN)]PF$_6$ (104 mg, 0.192 mmol) and eluted with acetonitrile (35 mL). This anion exchange process was repeated twice, after which the resulting liquid was purified by passing it twice through a short plug of alumina (eluent: acetonitrile). The product was then vacuum-dried overnight. The desired product was obtained as a dark brown solid (122 mg, 94% yield). ^{1}H NMR (400 MHz, CD_3CN): δ = 0.92 (t, 3H, CH_3, J = 6.93 Hz), 1.26–1.40 (m, 6H, C_3H_6), 1.96 (s, 3H, $NCCH_3$), 2.01–2.12 (m, 2H, NCH_2CH_2), 4.16–4.52 (m, 2H, NCH_2), 4.45 (s, 5H, C_5H_5), 7.46–7.51 (m, 1H, 5-Pyr-CH), 7.90–7.97 (m, 2H, 3,4-Pyr-CH), 8.60 (s, 1H, N=CH), 9.38 (d, 1H, 6-Pyr-CH, J = 5.50 Hz). ^{19}F NMR (400 MHz, CD_3CN): δ = –80.24. FT-IR (ATR, cm^{-1}): 570, 599, 613, 653, 739, 763, 787, 835, 921, 993,

1053, 1099, 1134, 1177, 1225, 1296, 1331, 1348, 1439, 1469, 1550, 1608, 2860, 2932. Anal. Calcd. for $C_{21}H_{26}F_6N_4O_4RuS_2$: C, 37.22; H, 3.87; N, 8.27. Found: C, 37.43; H, 4.16; N, 8.11.

Synthesis of [Ru(Cp)L^1(CO)]Tf$_2$N (1-CO). A solution of **1-MeCN** (50 mg, 0.019 mmol) in dichloromethane (5 mL) was stirred at ambient temperature for 16 h under CO atmosphere. The solvent was removed under reduced pressure, the residue was dissolved in acetonitrile and passed through a short plug of alumina (eluent: acetonitrile), and the product was dried under vacuum for 6 h. The desired product was obtained as a yellow liquid (43 mg, 87% yield). ^{1}H NMR (400 MHz, CD_3CN): δ = 0.90 (t, 3H, CH_3, J = 6.73 Hz), 1.26–1.39 (m, 8H, C_4H_8), 4.07 (t, 2H, NCH_2, J = 7.01 Hz), 5.23 (s, 5H, C_5H_5), 7.48–7.55 (m, 1H, 5-Pyr-CH), 8.05–8.13 (m, 2H, 3,4-Pyr-CH), 8.54 (s, 1H, N=CH), 8.99 (d, 1H, 6-Pyr-CH, J = 5.48 Hz). FT-IR (ATR, cm^{-1}): 559, 569, 599, 613, 652, 739, 770, 839, 1052, 1134, 1179, 1225, 1330, 1347, 1475, 1595, 1693, 1971 (CO), 2861, 2932, 3113. Anal. Calcd. for $C_{20}H_{23}F_6N_3O_5RuS_2$: C, 36.15; H, 3.49; N, 6.32. Found: C, 36.45; H, 3.75; N, 6.32.

Synthesis of [Ru(Cp)L^1(L)]Tf$_2$N (1-L; L = SMe$_2$ or DMSO). A solution of **1-MeCN** (50 mg, 0.019 mmol) in dimethyl sulfide (2.5 mL) was stirred at ambient temperature for 4 h. Then, the solvent was removed under reduced pressure, and the product was dried under vacuum for 4 h. The desired compound (**1-SMe$_2$**) was obtained quantitatively as a dark brown viscous liquid. ^{1}H NMR (400 MHz, $CDCl_3$): δ = 0.93 (t, 3H, CH_3, J = 7.05 Hz), 1.31–1.48 (m, 6H, C_3H_6), 1.79 (s, 6H, SCH_3), 1.83–2.04 (m, 2H, NCH_2CH_2), 4.25–4.42 (m, 2H, NCH_2), 4.55 (s, 5H, C_5H_5), 7.46 (ddd, 1H, 5-Pyr-CH, J = 1.46, 6.59, 7.73 Hz), 7.89 (td, 1H, 4-Pyr-CH, J = 1.38, 7.74 Hz), 8.10 (d, 1H, 3-Pyr-CH, J = 7.87 Hz), 8.71 (s, 1H, N=CH), 9.23 (d, 1H, 6-Pyr-CH, J = 5.45 Hz). FT-IR (ATR, cm^{-1}): 569, 599, 613, 652, 739, 767, 786, 834, 973, 1052, 1134, 1178, 1225, 1348, 1432, 1468, 1542, 1605, 2860, 2928. Anal. Calcd. for $C_{21}H_{29}F_6N_3O_4RuS_3$: C, 36.10; H, 4.18; N, 6.01. Found: C, 35.99; H, 4.07; N, 6.02. This compound gradually changed to **1-CD$_3$CN** when dissolved in CD_3CN. **1-DMSO** was

prepared by the same method as that using DMSO and was obtained quantitatively as a dark brown solid after drying under vacuum for 6 h at 353 K. ^{1}H NMR (400 MHz, CD_3CN): δ = 0.93 (t, 3H, CH_3, J = 7.10 Hz), 1.29–1.50 (m, 6H, C_3H_6), 2.11 (m, 2H, NCH_2CH_2), 2.86 (s, 3H, $O=S(CH_3)_2$), 3.16 (s, 3H, $O=S(CH_3)_2$), 4.26–4.32 (m, 2H, NCH_2), 4.80 (s, 5H, C_5H_5), 7.47–7.52 (m, 1H, 5-Pyr-CH), 7.97–8.04 (m, 2H, 3,4-Pyr-CH), 8.57 (s, 1H, N=CH), 9.21 (d, 1H, 6-Pyr-CH, J = 5.52 Hz). FT-IR (ATR, cm^{-1}): 569, 612, 652, 688, 739, 776, 837, 925, 965, 1010, 1052, 1077, 1134, 1180, 1224, 1331, 1348, 1417, 1471, 1611, 2862, 2930. Anal. Calcd. for $C_{21}H_{29}F_6N_3O_5RuS_3$: C, 35.29; H, 4.09; N, 5.88. Found: C, 35.31; H, 4.04; N, 5.78.

Synthesis of [Ru(Cp)L^2(CO)]PF$_6$. An acetonitrile solution (10 mL) of L^2 (64 mg, 0.31 mmol) was added to $[Ru(Cp)(MeCN)_3]PF_6$ (99 mg, 0.23 mmol) under nitrogen atmosphere and stirred for 3 h under dark. The solution was then passed through a short plug of alumina (eluent: acetonitrile) and stirred overnight at room temperature under CO atmosphere, during which the solution turned from brown to yellow. After solvent removal, the residue was washed thrice with diethyl ether (5 mL) to remove the unreacted ligand. Further, the product was dried under vacuum overnight. The desired product was obtained as a yellow solid (109 mg, 87% yield). ^{1}H NMR (400 MHz, CD_3CN): δ = 0.87–0.95 (m, 3H, CH_3), 1.24–1.39 (m, 6H, C_3H_6), 2.08–2.12 (m, 2H, NCH_2CH_2), 2.77, 2.78 (s, 3H, NCH_3), 2.91–3.16 (m, 2H, $NCH_2C_5H_{11}$), 3.98–4.41 (m, 2H, NCH_2–Pyr), 5.12, 5.17 (s, 5H, C_5H_5), 7.31–7.38 (m, 1H, 5-Pyr-CH), 7.55–7.62 (m, 2H, 3-Pyr-CH), 7.92–7.98 (m, 1H, 4-Pyr-CH), 8.67–8.76 (m, 1H, 6-Pyr-CH). FT-IR (ATR, cm^{-1}): 555, 576, 589, 739, 775, 826, 902, 998, 1031, 1108, 1162, 1298, 1374, 1421, 1452, 1471, 1610, 1959 (CO), 2857, 2927, 3120. Anal. Calcd. for $C_{19}H_{27}F_6N_2OPRu$: C, 41.84; H, 4.99; N, 5.13. Found: C, 41.77; H, 5.11; N, 5.02.

Synthesis of [Ru(Cp)(CO)L^2]Tf$_2$N (2-CO). An anion exchange resin (Dowex 1X8, 7.5 g), charged with Tf_2N anion using an aqueous solution of KTf_2N, was placed in a column and eluted with acetonitrile (100 mL). The column was then charged with an acetonitrile solution

(5 mL) of $[Ru(Cp)L^2(CO)]PF_6$ (80 mg, 0.147 mmol) and eluted with acetonitrile. This anion exchange process was repeated twice, after which the resulting liquid was purified by passing twice through a short plug of alumina (eluent: acetonitrile), and the product was dried under vacuum overnight to yield the desired product as a brown liquid (100 mg, quantitative yield). ^{1}H NMR (400 MHz, CD_3CN): δ = 0.86–0.95 (m, 3H, CH_3), 1.24–1.39 (m, 6H, C_3H_6), 2.08–2.12 (m, 2H, NCH_2CH_2), 2.77, 2.78 (s, 3H, NCH_3), 2.90–3.16 (m, 2H, $NCH_2C_5H_{11}$), 3.98–4.41 (m, 2H, NCH_2–Pyr), 5.12, 5.17 (s, 5H, C_5H_5), 7.31–7.37 (m, 1H, 5-Pyr-CH), 7.55–7.62 (m, 2H, 3-Pyr-CH), 7.92–7.98 (m, 1H, 4-Pyr-CH), 8.67–8.76 (m, 1H, 6-Pyr-CH). ^{19}F NMR (400 MHz, CD_3CN): δ = –80.24. FT-IR (ATR, cm^{-1}): 570, 600, 614, 653, 739, 762, 787, 841, 1052, 1133, 1178, 1226, 1330, 1347, 1422, 1470, 1611, 1956 (CO), 2861, 2934. Anal. Calcd. for $C_{21}H_{27}F_6N_3O_5RuS_2$: C, 37.06; H, 4.00; N, 6.17. Found: C, 36.06; H, 3.76; N, 5.90.

Chemical reactivities

The thermal ligand desorption of **1-MeCN** was examined by heating it at 373 K under a vacuum for 3 h. The product was dissolved in CD_3CN under argon atmosphere, and an insoluble decomposition product was removed by filtration. The solution contained unreacted **1-MeCN** and **1-CD_3CN** in a 6:4 ratio, as revealed by ^{1}H NMR. The latter component originated from the 16-electron complex produced by MeCN desorption. When the thermally treated sample was exposed to the air before dissolution in CD_3CN, the decomposition of the 16-electron complex occurred, similar to $[Ru(Cp)(tmeda)]^+$.[13]

The interconversion between the ILs was investigated as follows: **1-CO** was dissolved in excess MeCN or SMe_2 and photoirradiated with UV light (365 nm, LED) for 5 min. Subsequently, the solvent was removed under reduced pressure to yield **1-MeCN** and **1-SMe_2** quantitatively, whereas photoirradiation for a long time produced impurity, as confirmed by

^{1}H NMR analysis. Similarly, photoirradiation of **1-CO** in DMSO quantitatively produced **1-DMSO**, though excess solvent removal required vacuum drying at 353 K in this case. Liquids of **1-L** (L = MeCN, DMSO, SMe_2), painted on a glass plate above their melting points, was placed under CO atmosphere in the dark. The ligand exchange gradually occurred to produce **1-CO**, concomitant with a color change to orange; the reactions of liquid **1-MeCN** and **1-DMSO** performed at 343 and 363 K, respectively, completed within several hours, whereas no reactions occurred in the solid state. **1-SMe$_2$** underwent the reaction at 290 K in two days. The dissociated ligands can be removed by vacuum drying.

X-ray crystallography

Single crystals of $[Ru(Cp)L^1(MeCN)]PF_6$ obtained by the slow cooling of an acetonitrile solution (233 K) were used for structural characterization. Diffraction data were collected using Bruker APEX II Ultra (source: Mo Kα) at 90 K, and SHELXL was used for analysis.[21] The Cp ring in the cation was refined as twofold disordered by rotation (occupancy ratio 0.62:0.38). Crystallographic parameters are listed in Table S1†. CCDC 2217910 contains the crystallographic data of this compound.

Conflicts of interest

There are no conflicts to declare.

Acknowledgments

We thank R. Inoue (Kobe Univ.) for his assistance with the TG-DTA measurements and photoirradiation experiments. This work was financially supported by the JSPS KAKENHI Grant-in-Aid for Transformative Research Areas (A) “Supra-ceramics” (grant number JP23H04629) and JSPS KAKENHI (grant number JP20H02756).

REFERENCES

1 (a) R. M. Moriarty, U. S. Gill and Y. Y. Ku, *J. Organomet. Chem.*, 1988, **350**, 157–190; (b) J. W. Walton and L. A. Wilkinson, π-Coordinated arene metal complexes and catalysis, in *Organometallic Chemistry*: *Volume 42*, ed. N. J. Patmore and P. I. P. Elliott, The Royal Society of Chemistry, 2018, vol. 42, pp. 125-171; (c) D. S. Perekalin and A. R. Kudinov, *Coord. Chem. Rev.*, 2014, **276**, 153–173.

2 (a) M. Zeng, L. Li and S. B. Herzon, *J. Am. Chem. Soc.*, 2014, **136**, 7058–7067; (b) M. D. Mbaye, B. Demerseman, J.-L. Renaud and C. Bruneau, *J. Organomet. Chem.*, 2005, **690**, 2149–2158; (c) M. Ito and T. Ikariya, *J. Synth. Org. Chem., Jpn.*, 2008, **66**, 1042–1048; (d) B. del Klerk-Engels, J. G. P. Delis, J.-M. Ernsting, C. J. Elsevier, H.-W. Frühauf, D. J. Stufkens, K. Vrieze, K. Goubitz and J. Fraanje, *Inorg. Chim. Acta*, 1995, **240**, 273–284; (e) G. G. A. Balavoine, T. Boyer and C. Livage, *Organometallics*, 1992, **11**, 456–459; (f) T. Achard, L. Egger, C. Tortoreto, L. Guénée and J. Lacour, *Helv. Chim. Acta*, 2020, **103**, e2000190; (g) D. DiMondo, M. E. Thibault, J. Britten and M. Schlaf, *Organometallics*, 2013, **32**, 6541–6554.

3 M. Kar, K. Matuszek and D. R. MacFarlane, Ionic Liquids, in *Kirk-Othmer Encyclopedia of Chemical Technology*, John Wiley & Sons, Inc., 2019.

4 (a) N. R. Brooks, S. Schaltin, K. Van Hecke, L. Van Meervelt, K. Binnemans and J. Fransaer, *Chem. – Eur. J.*, 2011, **17**, 5054–5059; (b) M. Iida, C. Baba, M. Inoue, H. Yoshida, E. Taguchi and H. Furusho, *Chem. – Eur. J.*, 2008, **14**, 5047–5056; (c) P. Zhang, Y. Gong, Y. Lv, Y. Guo, Y. Wang, C. Wang and H. Li, *Chem. Commun.*, 2012, **48**, 2334–2336; (d) S. A. Pierson, O. Nacham, K. D. Clark, H. Nan, Y. Mudryk and J. L. Anderson, *New J. Chem.*, 2017, **41**, 5498–5505; (e) D. Prodius and A.-V. Mudring, *Coord. Chem. Rev.*, 2018, **363**, 1–16.

5 (a) T. Tominaga and T. Mochida, *Chem. – Eur. J.*, 2018, **24**, 6239–6247; (b) Y. Funasako, T. Mochida, K. Takahashi, T. Sakurai and H. Ohta, *Chem. – Eur. J.*, 2012, **18**, 11929–11936.

6 (a) S. J. Osborne, S. Wellens, C. Ward, S. Felton, R. M. Bowman, K. Binnemans, M. Swadźba-Kwaśny, H. Q. N. Gunaratne and P. Nockemann, *Dalton Trans.*, 2015, **44**, 11286–11289; (b) Y. Yoshida and G. Saito, Progress in Paramagnetic Ionic Liquids, in *Ionic Liquids: Theory, Properties, New Approaches*, ed. A. Kokorin, IntechOpen, 2011, pp. 723–738.

7 T. Mochida, *Chem. Rec.*, 2023, **23**, e202300041.

8 (a) R. Sumitani, H. Yoshikawa and T. Mochida, *Chem. Commun.*, 2020, **56**, 6189–6192; (b) T. Ueda, T. Tominaga, T. Mochida, K. Takahashi and S. Kimura, *Chem. – Eur. J.*, 2018, **24**, 9490–9493; (c) A. Komurasaki, Y. Funasako and T. Mochida, *Dalton Trans.*, 2015, **44**, 7595–7605; (d) T. Inagaki, T. Mochida, M. Takahashi, C. Kanadani, T. Saito and D. Kuwahara, *Chem. – Eur. J.*, 2012, **18**, 6795–6804; (e) Y. Funasako, T. Inagaki, T. Mochida, T. Sakurai, H. Ohta, K. Furukawa and T. Nakamura, *Dalton Trans.*, 2013, **42**, 8317–8327.

9 T. Inagaki, K. Abe, K. Takahashi and T. Mochida, *Inorg. Chim. Acta*, 2015, **438**, 112–117.

10 T. Inagaki and T. Mochida, *Chem. – Eur. J.*, 2012, **18**, 8070–8075.

11 S. Mori and T. Mochida, *Organometallics*, 2013, **32**, 780–787.

12 T. Mochida, S. Maekawa and R. Sumitani, *Inorg. Chem.*, 2021, **60**, 12386–12391.

13 C. Gemel, J. C. Huffman, K. G. Caulton, K. Mauthner and K. Kirchner, *J. Organomet. Chem.*, 2000, **593–594**, 342–353.

14 (a) D. Turnbull and M. H. Cohen, Crystallization Kinetics and Glass Formation, in *Modern Aspects of the Vitreous State*, ed. J. D. MacKenzie, Butterworth, London, 1960; (b) L.-M. Wang, C. A. Angell and R. Richert, *J. Chem. Phys.*, 2006, **125**, 074505.

15 T. Makino, M. Kanakubo, Y. Masuda, T. Umecky and A. Suzuki, *Fluid Phase Equilib.*, 2014, **362**, 300–306.

16 G. S. Fulcher, *J. Am. Ceram. Soc.*, 1925, **8**, 789–794.

17 E. N. D. C. Andrade, *Nature*, 1930, **125**, 309–310.

18 (a) A. E. Pierri, A. Pallaoro, G. Wu and P. C. Ford, *J. Am. Chem. Soc.*, 2012, **134**, 18197–18200; (b) I. Chakraborty, J. Jimenez, W. M. C. Sameera, M. Kato and P. K. Mascharak, *Inorg. Chem.*, 2017, **56**, 2863–2873; (c) M. Wang, K. Murata, Y. Koike, G. Jonusauskas, A. Furet, D. M. Bassani, D. Saito, M. Kato, Y. Shimoda, K. Miyata, K. Onda and K. Ishii, *Chem. – Eur. J.*, 2022, **28**, e202200716.

19 P. Sudhindra, S. Ajay Sharma, N. Roy, P. Moharana and P. Paira, *Polyhedron*, 2020, **192**, 114827.

20 (a) R. Kakehashi, N. Tokai, T. Kohno, Y. Nakatsuji, S. Yamamura and G. Karlsson, *J. Oleo Sci.*, 2013, **62**, 123–132; (b) P. K. Srivastava and V. Choudhary, *J. Appl. Polym. Sci.*, 2012, **125**, 31–37.

21 G. M. Sheldrick, *Acta Crystallogr. Sect. A: Found. Adv.*, 2008, **64**, 112–122.

Table of Contents

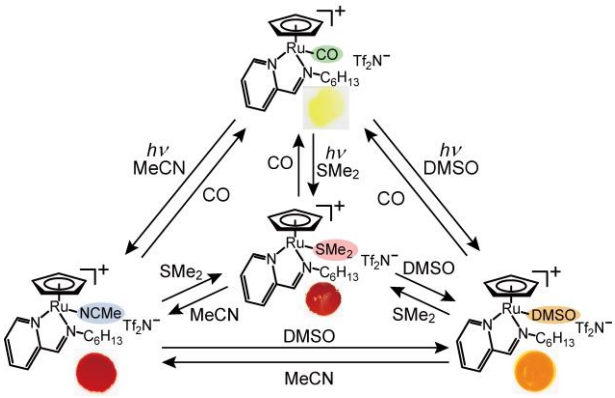

Ionic liquids with cationic half-sandwich ruthenium complexes with various auxiliary ligands have been synthesized. They undergo interconversion through in-situ ligand exchange, either photochemically or thermally.

Supporting Information

Ionic liquids containing half-sandwich ruthenium complexes: in-situ interconversions via photochemical and thermal ligand exchange

Tomoyuki Mochida,*[a,b] Syou Maekawa,[a] and Ryo Sumitani[a]

[a]*Department of Chemistry, Graduate School of Science, Kobe University, Rokkodai, Nada, Kobe, Hyogo 657-8501, Japan. E-mail: tmochida@platinum.kobe-u.ac.jp*
[b]*Research Center for Membrane and Film Technology, Kobe University, Rokkodai, Nada, Kobe, Hyogo 657-8501, Japan*

Contents

Fig. S1. ^{1}H NMR spectra of (a) **1-MeCN**, (b) **1-SMe$_2$**, and (c) **1-DMSO** (CD_3CN).

Fig. S2. ^{1}H NMR spectra of (a) **1-CO** and (b) **2-CO** (CD_3CN).

Fig. S3. Packing diagram of **1-MeCN** viewed along the *a*-axis.

Fig. S4. Simulated UV-vis spectra of **1-L** based on TD-DFT calculations.

Fig. S5. TG-DTA curves of **1-L** and **2-CO**.

Fig. S6. ^{1}H NMR spectra of **1-CO** before and after photoirradiation for 30 min (CD_3CN).

Fig. S7. Molecular orbitals of the cations in **1-L** and **2-CO** obtained by DFT calculations.

Table S1. Crystallographic parameters

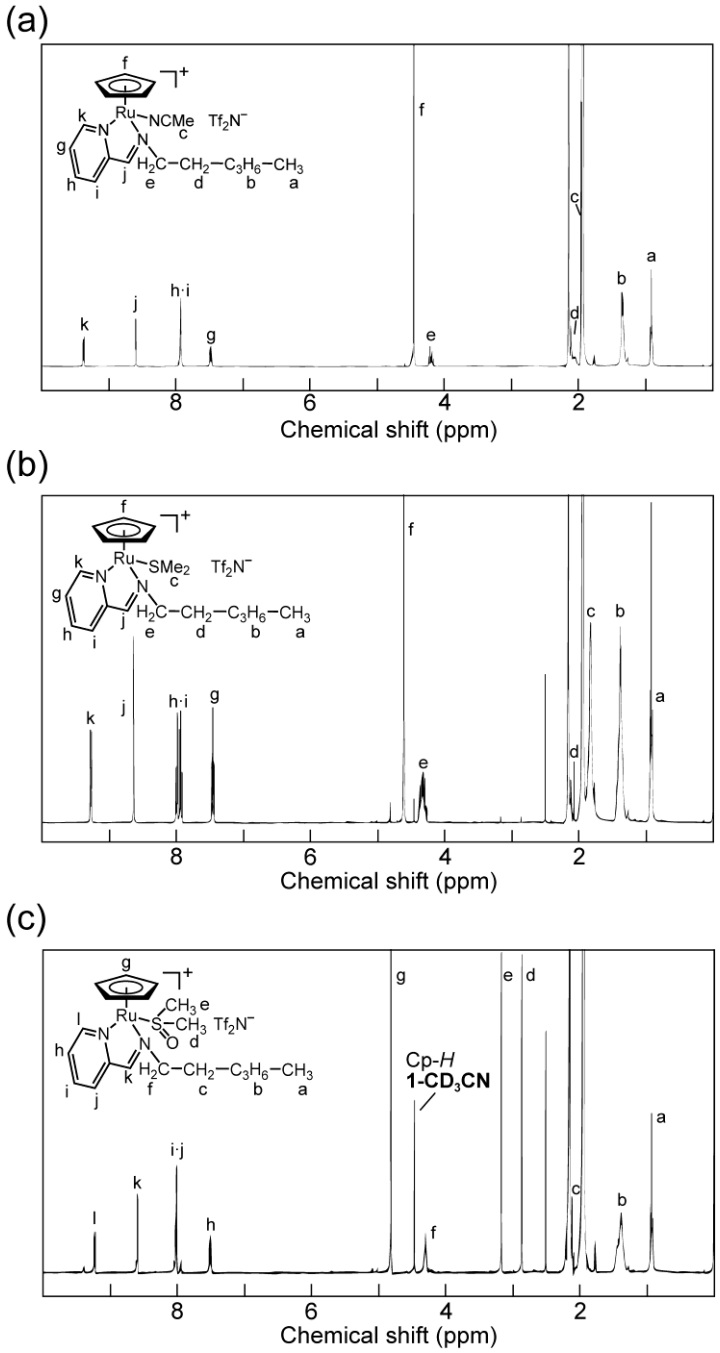

Figure S1. ^{1}H NMR spectra of (a) **1-MeCN**, (b) **1-SMe$_2$**, and (c) **1-DMSO** (in CD_3CN).

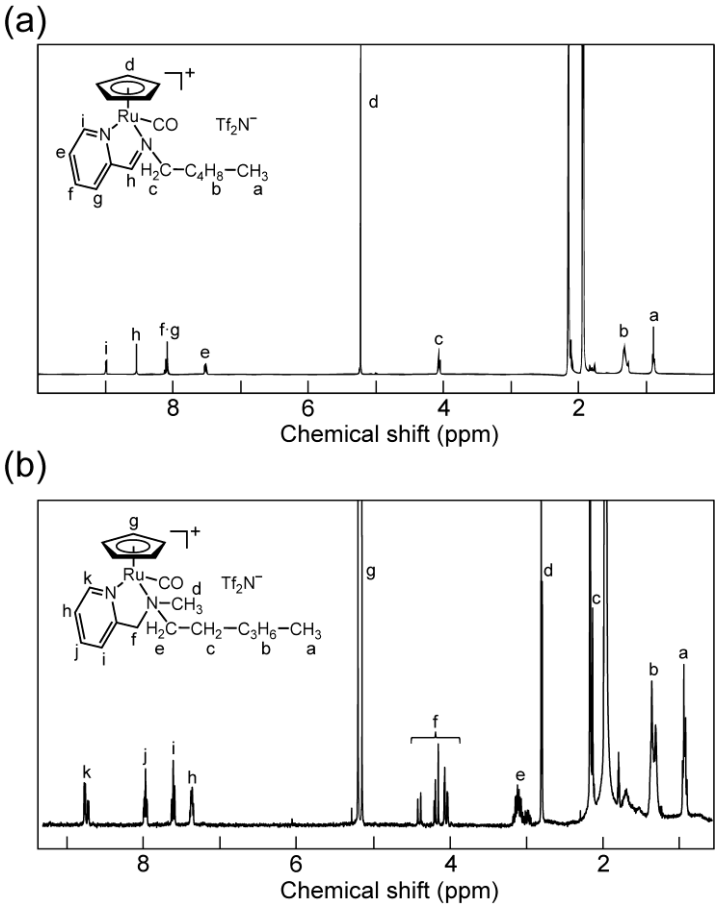

Figure S2. ^{1}H NMR spectra of (a) **1-CO** and (b) **2-CO** (in CD_3CN).

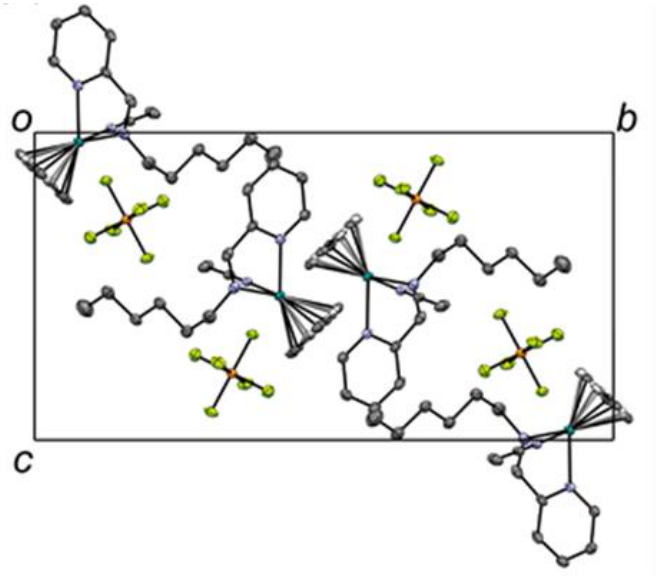

Figure S3. Packing diagram of **1-MeCN** viewed along the *a*-axis. Hydrogen atoms are omitted for clarity.

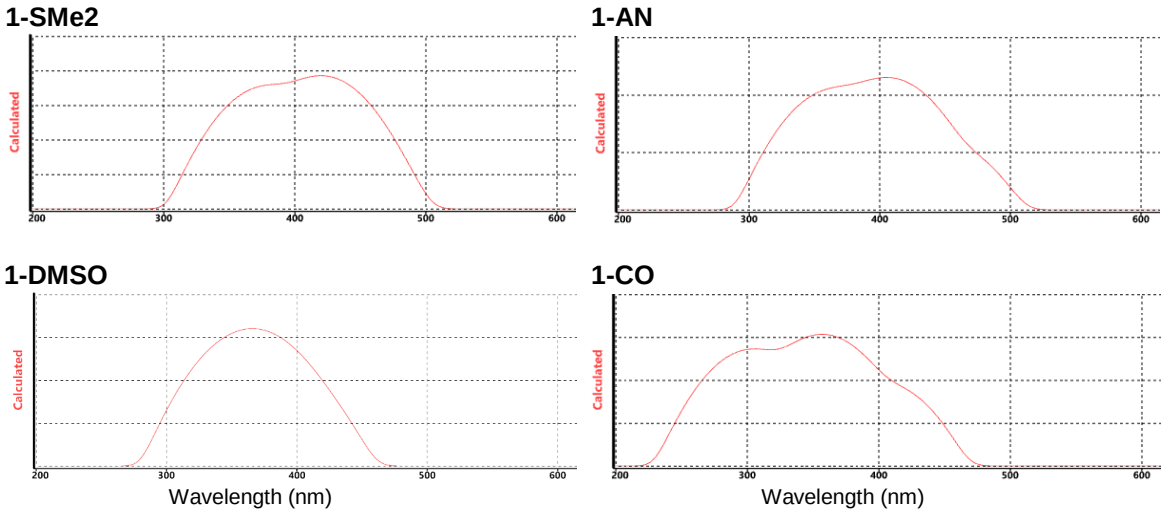

Figure S4. Simulated UV-vis spectra of **1-L** based on TD-DFT calculations.

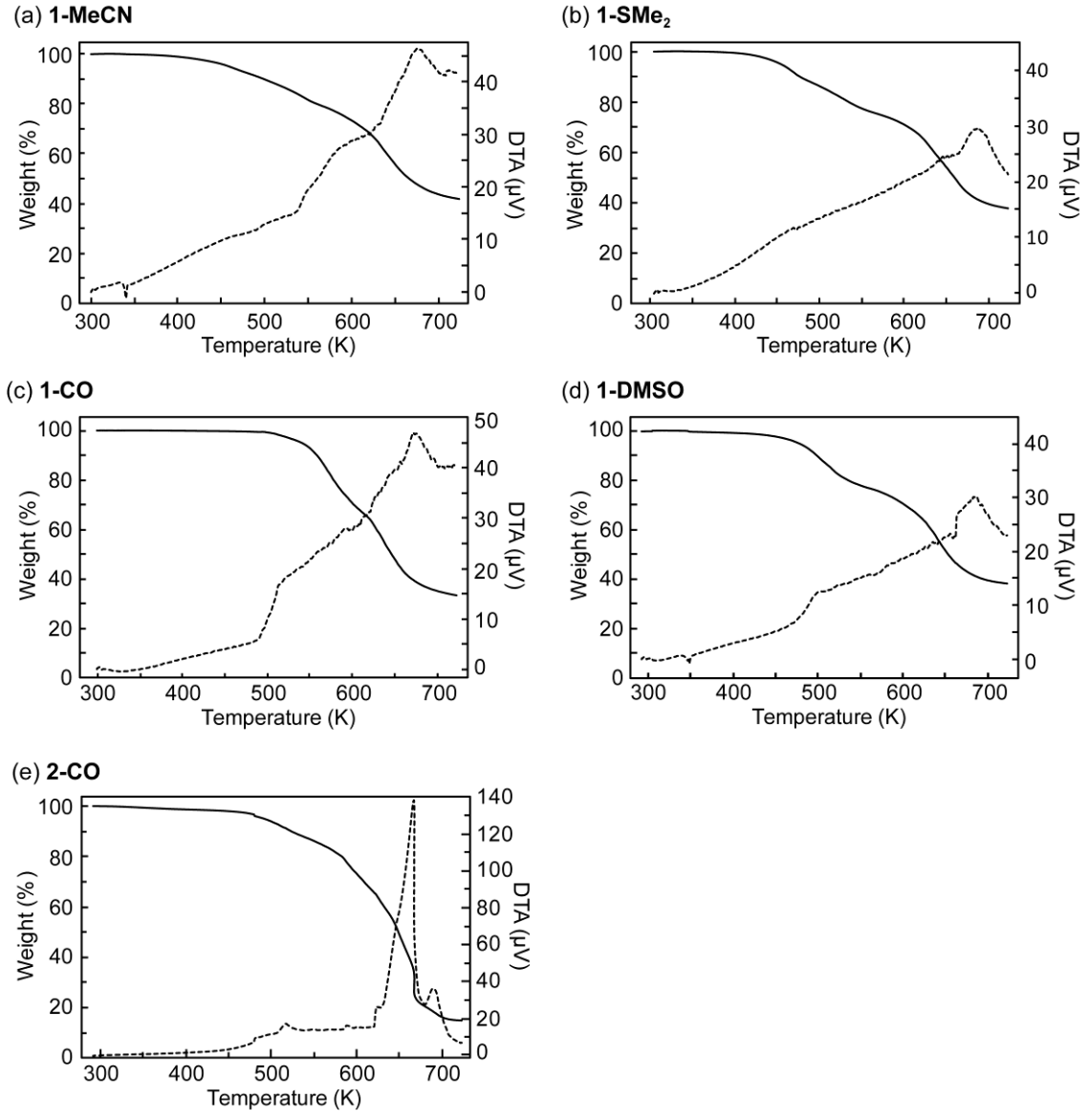

Figure S5. TG-DTA curves of **1-L** and **2-CO**.

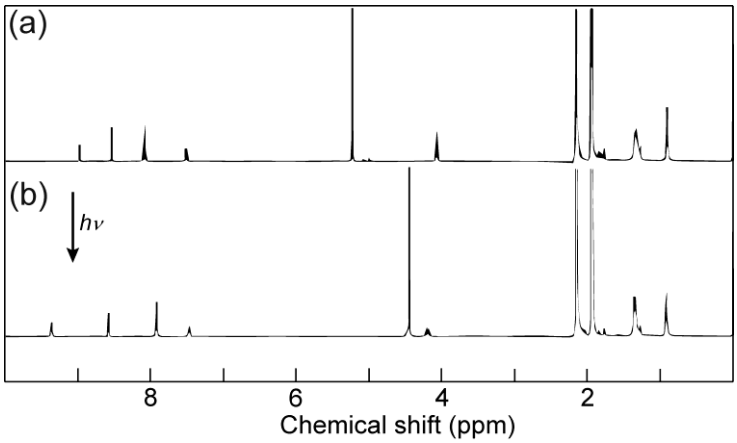

Figure S6. ^{1}H NMR spectra of **1-CO** before and after photoirradiation for 30 min (CD_3CN).

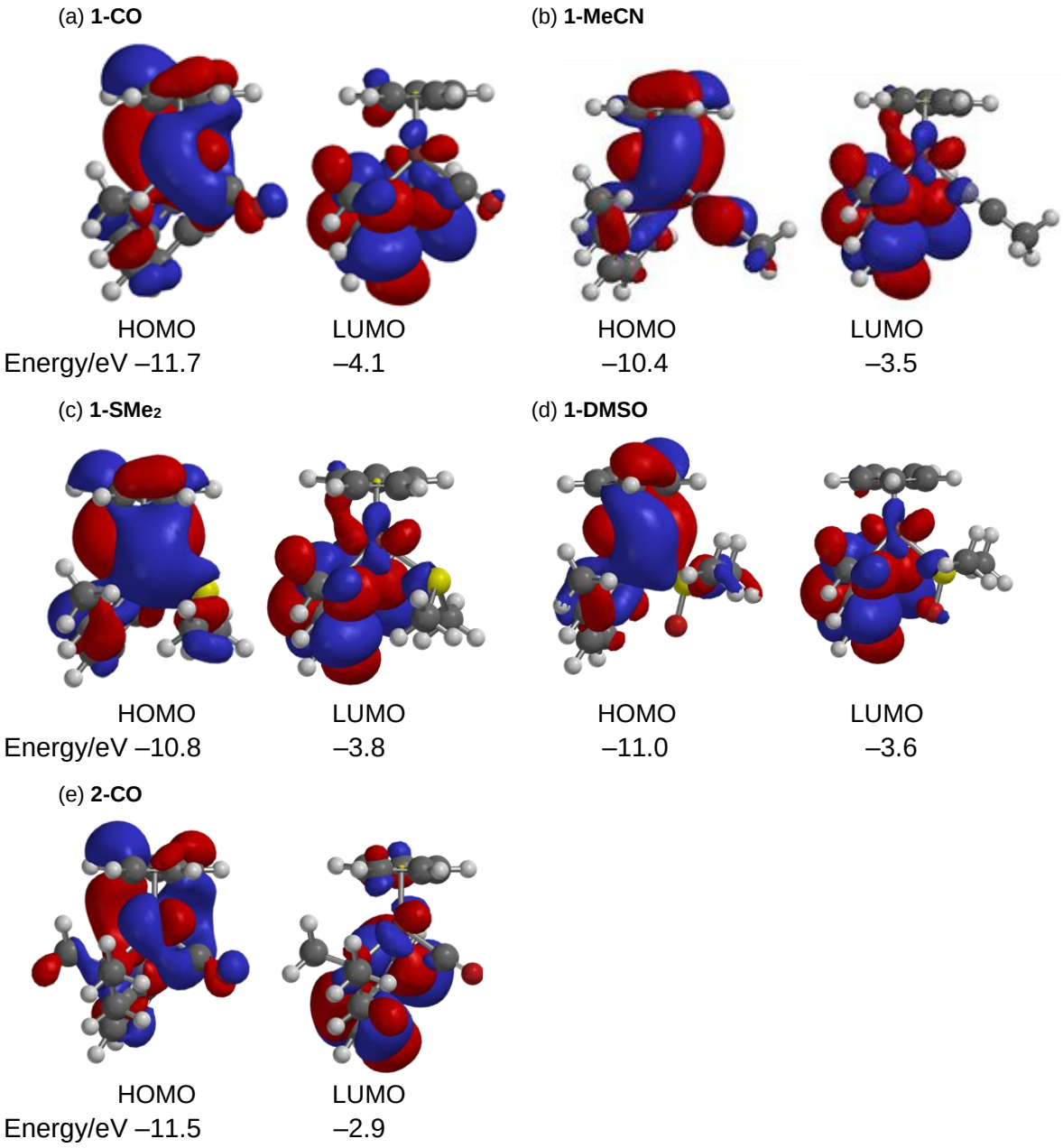

Figure S7. Molecular orbitals of the cations in **1-L** and **2-CO** obtained by DFT calculations.

Table S1. Crystallographic parameters

	[Ru(Cp)**L**^{1}(MeCN)]PF_6
Empirical formula	$C_{19}H_{26}F_6N_3PRu$
Formula weight	542.47
Crystal system	monoclinic
Space group	$P2_1/c$
a [Å]	9.4336(12)
b [Å]	21.056(3)
c [Å]	11.5841(14)
β [°]	104.669(2)
V [Å^3]	2226.0(5)
Z	4
ρ_{calcd} [g cm^{-3}]	1.619
F(000)	1096
Temperature [K]	90
Reflns collected	12833
Independent reflns	5085
Parameters	319
R_{int}	0.0446
$R_1{}^a$, $R_w{}^b$ ($I > 2\sigma(I)$)	0.0355, 0.0661
$R_1{}^a$, $R_w{}^b$ (all data)	0.0569, 0.0726
Goodness of fit	0.991
$\Delta\rho_{max,min}$ [e Å^{-3}]	0.519, –0.681
μ(Mo-Kα)	0.836

$^aR_1 = \Sigma||F_o| - |F_c|| / \Sigma|F_o|$. $^bR_w = [\Sigma w (F_o^2 - F_c^2)^2 / \Sigma w (F_o^2)^2]^{1/2}$